

Learning Interpretable Differentiable Logic Networks for Tabular Regression

Chang Yue and Niraj K. Jha

Abstract

Neural networks (NNs) achieve outstanding performance in many domains; however, their decision processes are often opaque and their inference can be computationally expensive in resource-constrained environments. We recently proposed Differentiable Logic Networks (DLNs) to address these issues for tabular classification based on relaxing discrete logic into a differentiable form, thereby enabling gradient-based learning of networks built from binary logic operations. DLNs offer interpretable reasoning and substantially lower inference cost.

We extend the DLN framework to supervised tabular regression. Specifically, we redesign the final output layer to support continuous targets and unify the original two-phase training procedure into a single differentiable stage. We evaluate the resulting model on 15 public regression benchmarks, comparing it with modern neural networks and classical regression baselines. Regression DLNs match or exceed baseline accuracy while preserving interpretability and fast inference. Our results show that DLNs are a viable, cost-effective alternative for regression tasks, especially where model transparency and computational efficiency are important.

1 Introduction

Interpretable neural architectures that integrate logical reasoning have gained increasing attention in recent years. Petersen *et al.* [1] first proposed *Deep Differentiable Logic Gate Networks* (LGNs), which relax the learning of conventional Boolean logic operations (e.g., AND, XOR) into differentiable forms, thereby enabling gradient-based learning of networks composed of logic gates. This strategy yields fast, interpretable models: the logic structure permits extraction of human-readable rules and the discrete implementation delivers highly efficient inference.

Building on this foundation, Petersen *et al.* [2] introduced *Convolutional Differentiable Logic Gate Networks*, adding deep logic-gate tree convolutions, logical-OR pooling, and residual initializations. These enhancements enable LGNs to exploit the convolution paradigm and scale to more complex classification tasks with improved accuracy. For example, their convolutional LGNs achieve 86.29% accuracy on CIFAR-10 with a model that is $29\times$ smaller than the previous state of the art.

Yue and Jha [3] restructured the LGN framework for general tabular classification, eliminating various constraints, such as fixed network topologies and binary-only inputs. The resulting *Differentiable Logic Networks* (DLNs) match or surpass standard NNs and LGNs on 20 public benchmarks while retaining interpretability and operating at several orders of magnitude lower computational cost than conventional multilayer perceptrons (MLPs).

Collectively, these studies establish logic-gate networks as a compelling alternative to conventional neural architectures in classification settings, combining transparency with efficiency.

Chang Yue and Niraj K. Jha are with the Department of Electrical and Computer Engineering, Princeton University, Princeton, NJ 08544, USA, e-mail: {cyue, jha}@princeton.edu.

This work was supported by the U.S. National Science Foundation under Grant CCF-2416541.

Despite these advances, existing logic-gate networks are limited to *classification*, predicting discrete class labels. Yet, many real-world applications in the scientific and industrial domains require *regression*, that is, predicting a continuous numerical output from input features. Current DLN architectures cannot be applied directly to such problems because they generate class scores or probabilities rather than a single continuous value. For instance, a DLN classifier counts the number of learned logical rules that fire for each class and selects the class with the most activated rules. Consequently, there is strong motivation to extend the DLN paradigm beyond classification, enabling tabular regression while preserving the interpretability and speed advantages that distinguish DLNs.

In this paper, we introduce a regression-focused extension of DLNs. The core innovation is a new *SumLayer* that enables DLNs to output a continuous value from the final layer of logic neurons. Specifically, the binary outputs of the last hidden layer are linearly combined by a SumLayer that learns continuous weights, connecting those outputs to a single numerical node. Unlike prior DLN classifiers, which aggregate logic activations into discrete class counts or probabilities, our SumLayer computes a weighted sum of the activated rules, yielding a continuous prediction. This simple yet effective change allows DLNs to address regression tasks directly. Crucially, the model’s interpretability is preserved: each neuron in the last hidden layer still represents a logical rule learned through differentiable relaxation and the final output is an intelligible weighted sum of these binary evaluations. Logic gates and sparse connections retain the computational efficiency of earlier DLNs and the additional overhead for output summation is negligible. Thus, the proposed regression DLN inherits the strengths of its predecessors while broadening their applicability. A simplified regression DLN is shown in Fig. 1.

We empirically validate the proposed model on 15 benchmark tabular regression datasets. Across these tasks, the regression DLN achieves predictive accuracy comparable to state-of-the-art black-box models, despite its much smaller logical architecture.

The remainder of this paper is organized as follows. Section 2 reviews related work. Section 3 describes the regression DLN architecture and the SumLayer mechanism. Section 4 presents experimental results and analysis. Section 5 concludes with a summary of findings and directions for future research.

2 Related Work

This work on regression DLNs intersects with several active research areas in machine learning: differentiable models, interpretable AI systems, and efficient machine learning.

Differentiable Machine Learning: The core idea of making traditionally non-differentiable structures differentiable is to enable gradient-based optimization. Real-valued logic extends classical Boolean logic to operate on continuous values (typically between 0 and 1) rather than on discrete true/false statements [4–6]. Efforts to create differentiable decision trees [7, 8] or embed them within larger differentiable architectures [9–11] aim to pair the interpretability of tree structures with the representational power of deep learning. Differentiable modeling is also being explored as a bridge between machine learning and scientific computing, allowing domain knowledge and constraints to be integrated directly into the learning process [12–16]. Continuous relaxation techniques are pivotal in this context, transforming discrete operations into smooth, differentiable counterparts so that gradients can be computed reliably [17, 18]. Building on these principles, logic-gate-based neural networks have made rapid progress [1–3]. Our work extends this line of research to tabular regression tasks by introducing a differentiable logic-gate architecture capable of predicting continuous targets.

Interpretable Machine Learning: The quest for transparency has spurred extensive work on explaining the behaviour of black-box models. Popular post-hoc techniques include Local Interpretable Model-Agnostic Explanations (LIME) [19], Shapley Additive Explanations (SHAP) [20], saliency maps [21], feature visualization [22], and, for regression, partial dependence plots (PDPs) and

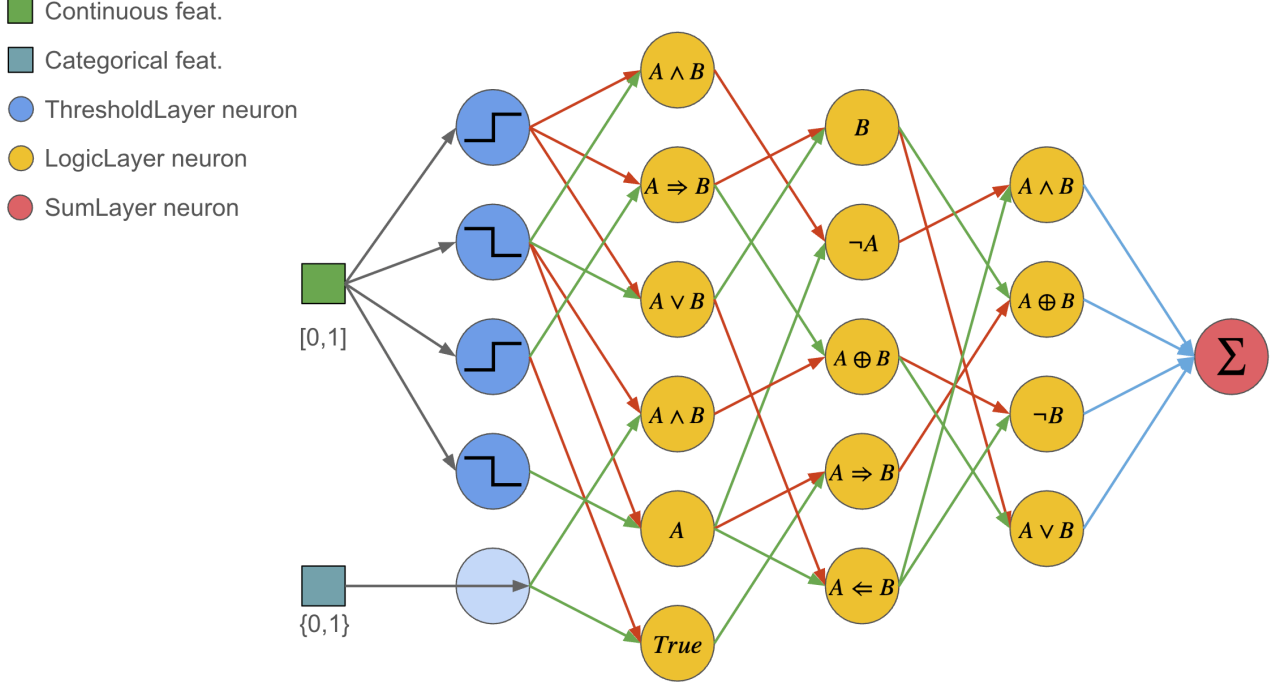


Figure 1: A simplified regression DLN example. Continuous input features are first binarized by a ThresholdLayer, producing a binary vector. This vector is then processed by successive LogicLayers composed of two-input Boolean operators. The activations of the final LogicLayer are combined by a SumLayer that computes a weighted sum, yielding the real-valued prediction.

individual conditional expectation (ICE) plots [23]. Post-hoc explanations, however, can be unreliable or even misleading [24], motivating the design of inherently interpretable models. Classical examples for regression include linear models and their regularised variants, Ridge and Lasso [25, 26], whose coefficients offer direct insight. More expressive, yet still transparent, approaches comprise Generalised Additive Models (GAMs) [27], which capture nonlinear effects additively, and rule-based systems such as RuleFit [28]. Broader interpretable structures include sparse decision trees [29] and scoring systems [30]. Neurosymbolic methods seek to fuse symbolic reasoning with neural representations. Logical Neural Networks (LNNs) [31] construct differentiable logic circuits with learnable weights but require a pre-specified logical skeleton, which may demand considerable domain expertise. Other efforts learn logic rules directly: Wang *et al.* [32] proposed the Rule-based Representation Learner, projecting rules into a continuous space and introducing Gradient Grafting for differentiation. Neural Logic Machines (NLMs) [33] perform multi-hop inference with iterative layers that approximate logical quantifiers, while Neural Logic Networks [34] dynamically build neural computation graphs from logical expressions and learn basic operations for propositional reasoning. Our regression DLN follows the same principle of end-to-end differentiability as the classification DLN but adapts the architecture to continuous targets. By learning weighted contributions from the final logic layer through a SumLayer, the model provides a transparent mapping from binary rule activations to the predicted value. The entire network remains optimizable with gradient descent while offering interpretability that is often missing from complex regression models.

Efficient Machine Learning: The aim of efficient machine learning is to reduce the computational and memory footprints of modern models, easing deployment on resource-constrained hardware, and lowering operational costs. Key strategies include network pruning, which removes redundant parameters or connections, to leave a sparse, lightweight subnetwork [35, 36]. Quantization further

shrinks models and can speed up inference by lowering the numerical precision of weights and activations. Extreme variants enable binary representations, as in Binarized Neural Networks (BNNs) [37] and XNOR-Net [38], while recent work focuses on large-model quantization techniques, such as Generative Pre-trained Transformer Quantization (GPTQ) [39, 40]. Knowledge distillation offers another route to efficiency: a small student network learns to mimic the outputs and internal representations of a larger teacher, yielding compact models that retain much of the teacher’s accuracy [41, 42]. Although these methods produce smaller and faster systems, they do not automatically enhance interpretability. Hardware specialization provides another avenue for speed and energy savings. Application-Specific Integrated Circuits (ASICs) and Field-Programmable Gate Arrays (FPGAs) deliver task-specific acceleration; for instance, Umuroglu *et al.* [43] and Petersen *et al.* [2] report substantial speed-ups for NNs on FPGAs. Because our models rely on simple logic operations and sparse connectivity, they align naturally with such hardware and can exploit these accelerators to achieve high efficiency without sacrificing interpretability.

3 Methodology

This section first offers a high-level overview of our approach and then details how each layer is trained. Four changes distinguish the proposed regression DLN from its classification predecessor. First, the SumLayer produces a floating-point weighted sum of logic activations rather than a discrete class-wise vote. Second, the network ends in a single-output neuron that outputs a real-valued prediction instead of one node per class. Third, neuron functions and connections are learned jointly in a single optimization stage, replacing the two-phase procedure used for classification DLNs. Fourth, every sigmoid and softmax employs a temperature parameter that is annealed during training, gradually sharpening the approximations to hard logical decisions.

Fig. 2 summarises the complete training workflow. First, we pre-process and discretize raw inputs; we then perform hyper-parameter optimization (HPO) under a fixed computational budget. Using the best hyper-parameters, we train the model end-to-end with gradient descent. Finally, we simplify the learned logic expressions and evaluate the resulting predictor.

Similar to classification DLNs, the regression DLN, as shown in Fig. 1, contains three layer types. A *ThresholdLayer* connected to the inputs binarizes continuous features into 0/1 values. One or more *LogicLayers* introduce nonlinearity through two-input Boolean operators. A final *SumLayer* aggregates the weighted activations of the last LogicLayer to produce a continuous output. Because the model’s prediction is an explicit weighted sum of binary rule evaluations, one can extract the underlying logic rules directly, making the network inherently interpretable. Unlike conventional MLPs, which rely on dense matrix multiplications, the DLN’s hidden layers execute only simple binary logic operations and each logic neuron receives inputs from exactly two neurons in the preceding layer. This operational simplicity and extreme sparsity result in highly efficient inference.

Training has two objectives: selecting the function each neuron implements and choosing the connections between layers. Discrete choices preclude straightforward gradient descent; hence, following the original DLN work, we relax both the neuron-function search and the connection search into continuous, differentiable optimizations. Whereas the classification DLN used a two-phase schedule—learning functions first and connections second, we find that regression benefits from a single unified phase in which both sets of parameters are optimized together, epoch by epoch. Concretely, we cast each decision as a classification problem: for every logic neuron, we learn logit weights whose softmax values represent a probability distribution over candidate logic functions and for every potential input pair, we learn logits that choose which two neurons feed a given neuron. During training, we anneal a temperature parameter applied to these logits, gradually sharpening soft probabilities into near-discrete choices. This temperature scheduling improves convergence and final accuracy in

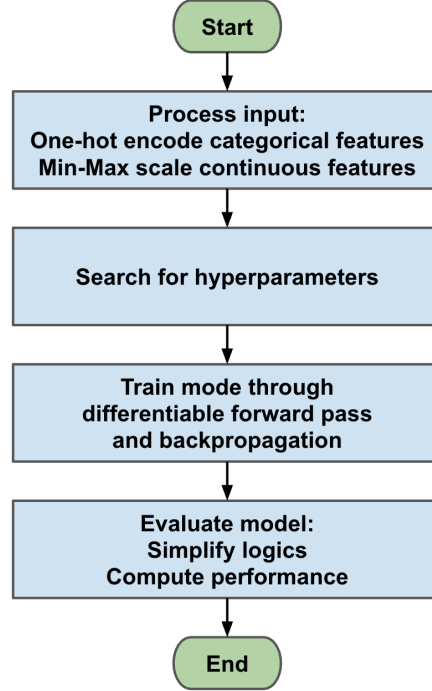


Figure 2: Training workflow for a regression DLN.

Table 1: Summary of DLN trainable parameters and feedforward functions during unified training and during inference. We use \mathbf{x} to denote input and \mathbf{y} to denote the output of each layer.

| | ThresholdLayer | LogicLayer | SumLayer |
|----------------------|---|--|--|
| Trainable parameters | bias $\mathbf{b} \in \mathbb{R}^{\text{in.dim}}$ slope $\mathbf{s} \in \mathbb{R}^{\text{in.dim}}$ | logic fn weight $\mathbf{W} \in \mathbb{R}^{\text{out.dim} \times 16}$ link a weight $\mathbf{U} \in \mathbb{R}^{\text{out.dim} \times \text{in.dim}}$ link b weight $\mathbf{V} \in \mathbb{R}^{\text{out.dim} \times \text{in.dim}}$ | link weight $\mathbf{S} \in \mathbb{R}^{\text{in.dim}}$ coefficient $\mathbf{C} \in \mathbb{R}^{\text{in.dim}}$ |
| Training | $\mathbf{y}_i = \text{Sigmoid}(\mathbf{s}_i \cdot (\mathbf{x}_i - \mathbf{b}_i) / \tau)$ | $\mathbf{y}_i = \sum_{k=0}^{15} P_k \text{SoftLogic}_k(a, b)$ $P = \text{Softmax}(\mathbf{W}_{i,:} / \tau)$ $a = \sum_{j=0}^{\text{in.dim}-1} [\text{Softmax}(\mathbf{U}_{i,:} / \tau)]_j \cdot \mathbf{x}_j$ $b = \sum_{j=0}^{\text{in.dim}-1} [\text{Softmax}(\mathbf{V}_{i,:} / \tau)]_j \cdot \mathbf{x}_j$ | $y = \sum_{j=0}^{\text{in.dim}-1} \text{Sigmoid}(\mathbf{S}_j / \tau) \cdot \mathbf{C}_j \cdot \mathbf{x}_j$ |
| Inference | $\mathbf{y}_i = \text{Heaviside}(\mathbf{s}_i \cdot (\mathbf{x}_i - \mathbf{b}_i))$ | $\mathbf{y}_i = \text{HardLogic}_k(\mathbf{x}_{a_i}, \mathbf{x}_{b_i})$ $k = \arg \max_j \mathbf{W}_{i,j}$ $a_i = \arg \max_j \mathbf{U}_{i,j}$ $b_i = \arg \max_j \mathbf{V}_{i,j}$ | $y = \sum_{j=0}^{\text{in.dim}-1} 1_{\{\text{Sigmoid}(\mathbf{S}_j / \tau) \geq \theta_{\text{sum-th}}\}} \cdot \mathbf{C}_j \cdot \mathbf{x}_j$ |

practice.

After training, we discretize all components, except the rule weights, to obtain a fully discrete DLN, as illustrated in Fig. 1. Although discretization can introduce quantization error, we mitigate this effect by employing straight-through estimators (STEs) during training, which keep the forward pass discrete while still allowing gradients to flow backward. This strategy aligns training and inference behaviors and preserves predictive accuracy, as discussed in Sec. 3.2.

Table 1 summarizes the trainable parameters for each layer type and explains their roles during training and inference. For clarity, we provide the forward-computation equations at the neuron

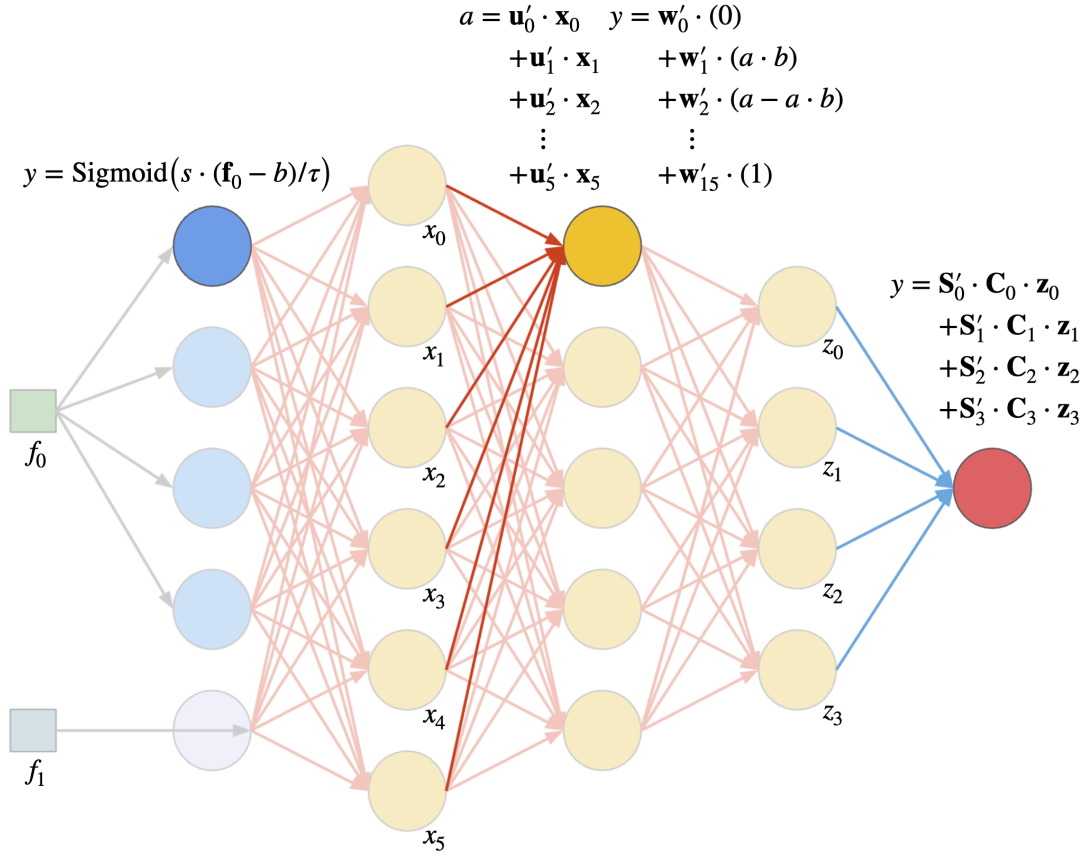


Figure 3: Illustration of the training process. The network learns neuron functions and connections simultaneously: key details are highlighted for clarity.

Algorithm 1 Training

Require: Training dataset \mathcal{D} , initial temperature τ , temperature decay rate γ , minimum temperature τ_{\min} , SumLayer link threshold $\theta_{\text{sum-th}}$

Ensure: Trained model parameters $\mathbf{b}, \mathbf{s}, \mathbf{W}, \mathbf{U}, \mathbf{V}, \mathbf{S}, \mathbf{C}$

```
1: for epoch = 1, 2, ..., E do
2:   for all  $(\mathbf{x}, z)$  in  $\mathcal{D}$  do
3:     {Forward pass}
4:     for layer in model_layers do
5:       if layer = ThresholdLayer then
6:         {Trainable parameters:  $\mathbf{b}, \mathbf{s}$ }
7:          $\mathbf{y}_i = \text{Sigmoid}(\mathbf{s}_i \cdot (\mathbf{x}_i - \mathbf{b}_i))$ 
8:       else if layer = LogicLayer then
9:         {Trainable parameters:  $\mathbf{W}, \mathbf{U}, \mathbf{V}$ }
10:         $\mathbf{P} = \text{Softmax}(\mathbf{W}_{i,:}/\tau)$ 
11:         $a = \sum_{j=0}^{\text{in\_dim}-1} [\text{Softmax}(\mathbf{U}_{i,:}/\tau)]_j \cdot \mathbf{x}_j$ 
12:         $b = \sum_{j=0}^{\text{in\_dim}-1} [\text{Softmax}(\mathbf{V}_{i,:}/\tau)]_j \cdot \mathbf{x}_j$ 
13:         $\mathbf{y}_i = \sum_{k=0}^{15} \mathbf{P}_k \cdot \text{SoftLogic}_k(a, b)$ 
14:      else
15:        {Trainable parameters:  $\mathbf{S}, \mathbf{C}$ }
16:         $\mathbf{y} = \sum_{j=0}^{\text{in\_dim}-1} \text{Sigmoid}(\mathbf{S}_j/\tau) \cdot \mathbf{C}_j \cdot \mathbf{x}_j$ 
17:      end if
18:       $\mathbf{x} = \mathbf{y}$  {Take preceding layer's output as input}
19:    end for
20:    {Backward pass}
21:    Compute loss  $\mathcal{L}(\mathbf{x}, z)$ 
22:    Backpropagate to compute gradients
23:    Update neuron function parameters  $\mathbf{b}, \mathbf{s}, \mathbf{W}$ 
24:     $\tau = \max(\tau \times \gamma, \tau_{\min})$  {Temperature decay}
25:  end for
26: end for
```

level—namely, how the i^{th} output \mathbf{y}_i is computed from the input vector \mathbf{x} .

ThresholdLayer. During inference, this layer employs the Heaviside step function; during training, it uses a scaled and shifted sigmoid to preserve differentiability.

LogicLayer. This layer learns both the Boolean operation performed by each neuron and the two incoming connections. Each candidate function or connection is associated with a learnable logit interpreted, after a softmax, as a probability. After training, every logit is quantized to its highest-probability discrete choice, yielding a fully logical circuit.

SumLayer. This layer contains (i) binary connection weights that specify which neurons in the previous layer contribute to the output and (ii) continuous coefficients that weight those contributions. At inference time, the connection weights are binarized, whereas the coefficients remain in floating-point format.

Fig. 3 illustrates the differentiable training process, in which neuron functions and connections are optimized simultaneously.

Algorithms 1 and 2 detail the training and inference procedures, respectively. For illustration, the pseudo-code assumes a mini-batch size of one and tracks how each neuron's output \mathbf{y}_i is generated at every layer. In practice, we train with a batch size of 32. Because the forward pass of every

Algorithm 2 Inference

Require: Input data \mathbf{x} **Require:** Model layer list $\begin{bmatrix} \text{ThresholdLayer} \\ \text{LogicLayer}_1 \\ \dots \\ \text{LogicLayer}_n \\ \text{SumLayer} \end{bmatrix}$

```
1: {First layer: ThresholdLayer}
2:  $\mathbf{y}_i = \text{Heaviside}(\mathbf{s}_i \cdot (\mathbf{x}_i - \mathbf{b}_i))$ 
3: {Middle layers: LogicLayer}
4: for  $l = 1, 2, \dots, n$  do
5:    $k = \arg \max_j \mathbf{W}_{i,j}$ 
6:    $a_i = \arg \max_j \mathbf{U}_{i,j}$ 
7:    $b_i = \arg \max_j \mathbf{V}_{i,j}$ 
8:    $\mathbf{x} = \mathbf{y}$  {Take preceding layer's output as input}
9:    $\mathbf{y}_i = \text{HardLogic}_k(\mathbf{x}_{a_i}, \mathbf{x}_{b_i})$ 
10: end for
11: {Last layer: SumLayer}
12:  $\hat{\mathbf{y}} = \sum_{j=0}^{\text{in\_dim}-1} 1_{\{\text{Sigmoid}(\mathbf{S}_j/\tau) \geq \theta_{\text{sum-th}}\}} \cdot \mathbf{C}_j \cdot \mathbf{y}_j$ 
13: return  $\hat{\mathbf{y}}$ 
```

layer is differentiable, gradient-based back-propagation proceeds automatically. We present additional mathematical details in the following subsections.

3.1 Unified End-to-End Optimization

We propose a single end-to-end optimization procedure for regression DLNs that simultaneously learns (i) the threshold parameters in the *ThresholdLayer*; (ii) the logical functions of neurons in the *LogicLayer*; (iii) the connection structure in both the *LogicLayer* and the *SumLayer*; and (iv) the rule coefficients in the *SumLayer*. Unlike prior work that splits these steps into separate training phases, our unified method updates all trainable parameters at once through continuous relaxations. Fig. 3 highlights the main components of this process. Next, we describe each layer's formulation and objective.

3.1.1 ThresholdLayer

This layer converts continuous inputs to binary features through a differentiable approximation of the Heaviside step. During training, each threshold neuron with input x has a learnable bias b and slope s and outputs

$$\begin{aligned} f(x) &= \text{Sigmoid}(s \cdot (x - b)/\tau) \\ &= \frac{1}{1 + e^{-[s \cdot (x - b)/\tau]}}, \end{aligned}$$

where τ is a temperature parameter shared across all sigmoid and softmax operations. At inference time, the neuron is discretized as

$$F(x) = \text{Heaviside}(s \cdot (x - b))$$

yielding a strict binary output. Temperature τ is annealed during training—an approach that markedly improves convergence for regression DLNs. A single threshold neuron's forward pass is depicted in

Fig. 3. The corresponding pseudo-code appears in lines 5–7 of Algorithm 1. The inference step is shown in line 2 of Algorithm 2.

Data preprocessing. Following the original DLN study, we apply min–max scaling to continuous variables and one-hot encoding to categorical variables so that every input lies in $[0, 1]$. Whereas classification DLNs allocate four or six threshold neurons per continuous feature, we find regression tasks benefit from greater resolution and use six or ten neurons instead.

Initialization. We set all slopes to $s = 2$, giving the sigmoids enough smoothness for informative gradients early in training, and initialize biases b from the bin edges of a decision-tree regressor fitted to each feature. After training, any bias that converges outside $[0, 1]$ is interpreted as a constant true or false, depending on the sign of s .

3.1.2 LogicLayer

Following LGN [1] and DLN [3], we employ *real-valued logic* to sidestep the non-differentiability of Boolean operators. As summarized in Table I of DLN [3], real-valued logic extends Boolean logic by mapping both inputs and outputs to the interval $[0, 1]$. We write SoftLogic_k for the differentiable form of the k^{th} operator and HardLogic_k for its Boolean counterpart. For example, the real-valued AND gate is

$$\begin{aligned}\text{real-valued AND}(a, b) &= \text{SoftLogic}_1(a, b) \\ &= a \cdot b,\end{aligned}$$

where $a, b \in [0, 1]$ are continuous real numbers. The Boolean gate used at inference time is

$$\begin{aligned}\text{binary AND}(a, b) &= \text{HardLogic}_1(a, b) \\ &= 1_{\{a=1\}} \cdot 1_{\{b=1\}},\end{aligned}$$

where $a, b \in \{0, 1\}$ are discrete binary numbers and indicator functions are applied to them. During training, we use SoftLogic_k (Algorithm 1, line 13); at inference time, we switch to HardLogic_k (Algorithm 2, line 9).

Each LogicLayer neuron realizes one of the 16 two-input Boolean functions. Following LGN [1], we represent the function choice with a learnable logit vector $\mathbf{w} \in \mathbb{R}^{16}$. Given scalar inputs a and b , the neuron’s output during training is

$$\begin{aligned}y &= \sum_{k=0}^{15} \left[\text{Softmax}(\mathbf{w}/\tau) \right]_k \cdot \text{SoftLogic}_k(a, b) \\ &= \sum_{k=0}^{15} \frac{e^{\mathbf{w}_k/\tau}}{\sum_j e^{\mathbf{w}_j/\tau}} \cdot \text{SoftLogic}_k(a, b),\end{aligned}$$

where τ is the global temperature.

Selecting the two incoming signals is another discrete choice. Each neuron therefore maintains two logit vectors $\mathbf{u}, \mathbf{v} \in \mathbb{R}^{\text{in.dim}}$, whose softmaxes pick weighted combinations of the previous layer’s outputs \mathbf{x} :

$$\begin{aligned}a &= \sum_{j=0}^{\text{in.dim}-1} \left[\text{Softmax}(\mathbf{u}/\tau) \right]_j \cdot \mathbf{x}_j, \\ b &= \sum_{j=0}^{\text{in.dim}-1} \left[\text{Softmax}(\mathbf{v}/\tau) \right]_j \cdot \mathbf{x}_j.\end{aligned}$$

These steps appear in Algorithm 1, lines 10–13, and are highlighted for one neuron in Fig. 3.

At inference time, we quantize to the arg-max choices:

$$\begin{aligned} k &= \arg \max_i \mathbf{w}_i, \\ a_i &= \arg \max_i \mathbf{u}_i, \\ b_i &= \arg \max_i \mathbf{v}_i, \\ y &= \text{HardLogic}_k(\mathbf{x}_{a_i}, \mathbf{x}_{b_i}). \end{aligned}$$

The corresponding pseudo-code is given in Algorithm 2, lines 5–9.

3.1.3 SumLayer

The SumLayer in the regression DLN diverges markedly from its counterpart in classification DLNs. Because a regression model outputs a single continuous value, the SumLayer computes a weighted sum of the activations from the preceding (final) LogicLayer. We leave the coefficients \mathbf{c} for these activations in floating-point format; only the binary connectivity pattern is later quantized. As in the original DLN, we represent the presence of each potential input connection with a learnable sigmoid gate. Concretely, for every candidate input \mathbf{x}_j , the layer maintains (i) a link-strength logit $\mathbf{s}_j \in \mathbb{R}$ and (ii) a continuous rule weight $\mathbf{c}_j \in \mathbb{R}$. Given the previous layer’s output vector \mathbf{x} , during training, the layer outputs

$$y = \sum_{j=0}^{\text{in.dim}-1} \text{Sigmoid}(\mathbf{s}_j/\tau) \cdot \mathbf{c}_j \cdot \mathbf{x}_j.$$

After training, we discretize the connection pattern by retaining links whose gate value exceeds a fixed threshold $\theta_{\text{sum-th}}$. The inference computation therefore becomes

$$y = \sum_{j=0}^{\text{in.dim}-1} 1_{\{\text{Sigmoid}(\mathbf{s}_j/\tau) \geq \theta_{\text{sum-th}}\}} \cdot \mathbf{c}_j \cdot \mathbf{x}_j.$$

where we set $\theta_{\text{sum-th}} = 0.8$, following DLN. The corresponding pseudo-code appears in line 16 of Algorithm 1 and line 12 of Algorithm 2.

3.2 Training Strategies and Model Simplification

To train regression DLNs effectively, we adapt several strategies originally introduced for classification DLNs [3]. We summarize these methods below and apply them analogously in our framework; readers seeking additional detail can consult the cited work.

- **Searching over Subspaces:** To curb the size of the search space for neuron functions and input links, we restrict each neuron to a subset of candidate gates and connections. We set the logits of excluded options to $-\infty$ inside the softmax, thereby focusing optimization on a manageable subspace and improving gradient flow.
- **Using Straight-Through Estimators (STEs):** Cascaded sigmoids and softmax operations can dull activations. We employ the STE [44] so that the forward pass uses discrete outputs while the backward pass propagates gradients from their continuous relaxations. This adjustment makes regression DLNs substantially more trainable.

Table 2: Characteristics of the datasets after preprocessing

| Dataset | # Train | # Test | # Cont. | # Cate. | Source | ID |
|-------------|---------|--------|---------|---------|--------|--|
| Abalone | 3132 | 1045 | 7 | 2 | UCI | 1 |
| Airfoil | 1127 | 376 | 5 | 0 | UCI | 291 |
| Bike | 13032 | 4345 | 6 | 14 | UCI | 275 |
| CCPP | 7145 | 2382 | 4 | 0 | UCI | 294 |
| Concrete | 753 | 252 | 8 | 0 | UCI | 165 |
| Electrical | 7500 | 2500 | 12 | 0 | UCI | 471 |
| Energy | 576 | 192 | 6 | 4 | UCI | 242 |
| Estate | 310 | 104 | 6 | 0 | UCI | 477 |
| Housing | 15324 | 5109 | 8 | 4 | Kaggle | camnugent/california-housing-prices |
| Infrared | 763 | 255 | 31 | 6 | UCI | 925 |
| Insurance | 1002 | 335 | 2 | 12 | Kaggle | mirichoi0218/insurance |
| MPG | 294 | 98 | 6 | 2 | UCI | 9 |
| Parkinson’s | 4406 | 1469 | 18 | 1 | UCI | 189 |
| Wine | 3988 | 1330 | 11 | 0 | UCI | 186 |
| Yacht | 231 | 77 | 6 | 0 | Kaggle | heitornunes/yacht-hydrodynamics-data-set |

- **Concatenating Inputs:** Inspired by the Wide & Deep model [45] and DLN, we concatenate the binarized inputs produced by the ThresholdLayer to the inputs of intermediate LogicLayers. This shortcut improves information flow, grants later layers direct access to raw features, and eases gradient propagation.
- **Model Simplification:** After training, we extract the learned logical expressions and simplify them with symbolic tools (e.g., SymPy [46]), mirroring the procedure in DLN. This step reduces model size and enhances interpretability.

We validate the effectiveness of these strategies through ablation studies whose results appear in Sec. 4.5.

Temperature Scheduling. Unlike the original DLN, our training employs an exponential temperature decay for every sigmoid and softmax. The temperature τ is initialized to a large value and multiplied by a factor $\gamma < 1$ after each epoch until it reaches a minimum τ_{\min} . The trio $(\tau, \gamma, \tau_{\min})$ is treated as a set of hyperparameters and tuned during experimentation.

4 Experiments

We evaluate the proposed DLN against nine baseline methods on 15 tabular regression datasets drawn from the UC Irvine Machine Learning Repository [47] and the Kaggle platform [48]. The baselines are linear regression, Ridge, Lasso, k -nearest neighbors (KNN), decision tree (DT), AdaBoost (AB), random forest (RF), support vector regression (SVR), and MLP. Table 2 lists each dataset’s characteristics after preprocessing; sample sizes range from hundreds to thousands. We assess predictive accuracy and inference cost, and we illustrate DLN’s interpretability by visualizing its decision process. As summarized in Fig. 4, DLN lies on the Pareto frontier under every experimental setting.

4.1 Experimental Setup

We preprocess each dataset as follows:

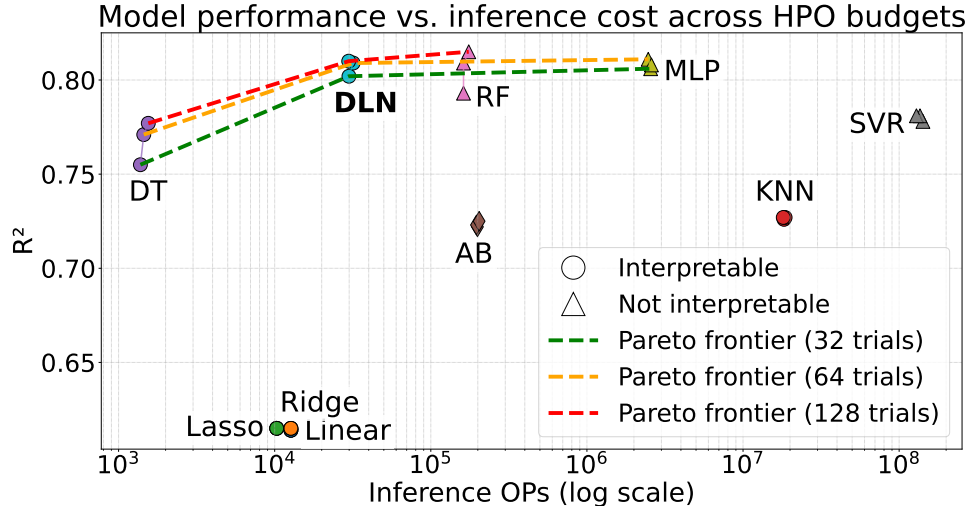


Figure 4: Comparison of R^2 and the number of operations required for inference across models. We plot results for 32, 64, and 128 hyperparameter-search trials and draw the Pareto frontier for each case; DLN is Pareto-optimal in all three.

1. Remove rows with missing values. The selected datasets are almost complete; hence, only a negligible number of rows are discarded.
2. One-hot encode categorical features.
3. Min-Max scale continuous features to the range $[0, 1]$.
4. Standardize targets to zero mean and unit variance.

For each dataset-model pair, we run 10 independent trials, each with a different random seed. Every trial comprises three stages: hyperparameter search, training, and evaluation. During hyperparameter search, we employ Optuna [49] to sample hyperparameter values from a predefined grid and select the value configuration that yields the lowest cross-validated mean-squared error (MSE). Depending on the dataset size, we use two to four folds, with smaller datasets receiving more folds. Data processing and all classical baselines rely on scikit-learn [50], whereas the MLP and DLN models are implemented in PyTorch [51]. Ray [52] orchestrates parallel hyperparameter searches and training runs.

4.2 Accuracy

The performance of the regression models is measured by three main metrics: R^2 , root-mean-square error (RMSE), and mean absolute error (MAE). We present the R^2 results in this section and provide the RMSE and MAE values in the Appendix. As expected, R^2 is strongly and inversely correlated with RMSE and MAE. Table 3 reports the average R^2 for all 10 models on the 15 datasets. Fig. 5 shows the full R^2 distribution for each model. DLN achieves the second-highest mean R^2 and the second-best average rank across all datasets, with random forest ranking first.

Linear regression and its two regularized variants, Ridge and Lasso, perform similarly but lack sufficient capacity for many tasks. KNN substantially improves over the linear models. Decision trees push the upper bound higher but are less stable. The boosting variant, AdaBoost, does not improve on a single tree, whereas the bagging variant, random forest, is robust—it attains a high peak and performs well on difficult datasets such as Parkinson’s and Wine. Support vector regression also

Table 3: Average test R^2 across 10 random seeds and 128 hyperparameter trials per model

| | Linear | Ridge | Lasso | KNN | DT | AB | RF | SVR | MLP | DLN |
|---------------------------|-------------------------------|-------------------------------|-------------------------------|-------------------------------|-------------------------------|-------------------------------|-------------------------------|-------------------------------|-------------------------------|-------------------------------|
| Abalone | 0.534 ± 0.024 | 0.534 ± 0.024 | 0.534 ± 0.024 | 0.517 ± 0.013 | 0.475 ± 0.018 | 0.463 ± 0.027 | 0.547 ± 0.019 | 0.551 ± 0.018 | 0.570 ± 0.024 | 0.526 ± 0.026 |
| Airfoil | 0.516 ± 0.034 | 0.516 ± 0.033 | 0.516 ± 0.033 | 0.874 ± 0.026 | 0.793 ± 0.052 | 0.743 ± 0.020 | 0.868 ± 0.016 | 0.822 ± 0.024 | 0.943 $\pm 5.7\text{e-}03$ | 0.889 ± 0.013 |
| Bike | 0.403 ± 0.012 | 0.403 ± 0.012 | 0.403 ± 0.012 | 0.659 ± 0.012 | 0.904 ± 0.011 | 0.660 ± 0.017 | 0.870 $\pm 7.1\text{e-}03$ | 0.645 ± 0.014 | 0.939 $\pm 3.0\text{e-}03$ | 0.916 $\pm 6.4\text{e-}03$ |
| CCPP | 0.929 $\pm 2.4\text{e-}03$ | 0.929 $\pm 2.4\text{e-}03$ | 0.929 $\pm 2.4\text{e-}03$ | 0.957 $\pm 2.0\text{e-}03$ | 0.942 $\pm 2.8\text{e-}03$ | 0.920 $\pm 3.8\text{e-}03$ | 0.947 $\pm 4.6\text{e-}03$ | 0.946 $\pm 2.2\text{e-}03$ | 0.948 $\pm 2.4\text{e-}03$ | 0.943 $\pm 2.3\text{e-}03$ |
| Concrete | 0.593 ± 0.034 | 0.593 ± 0.034 | 0.593 ± 0.034 | 0.709 ± 0.038 | 0.795 ± 0.029 | 0.791 ± 0.015 | 0.877 ± 0.018 | 0.869 ± 0.014 | 0.882 ± 0.022 | 0.888 ± 0.020 |
| Electrical | 0.647 ± 0.014 | 0.647 ± 0.014 | 0.647 ± 0.013 | 0.798 $\pm 4.0\text{e-}03$ | 0.755 ± 0.012 | 0.826 $\pm 8.4\text{e-}03$ | 0.843 ± 0.013 | 0.962 $\pm 1.7\text{e-}03$ | 0.968 $\pm 2.0\text{e-}03$ | 0.936 $\pm 3.6\text{e-}03$ |
| Energy | 0.911 $\pm 7.5\text{e-}03$ | 0.911 $\pm 7.5\text{e-}03$ | 0.911 $\pm 7.4\text{e-}03$ | 0.956 $\pm 9.0\text{e-}03$ | 0.995 $\pm 2.4\text{e-}03$ | 0.969 $\pm 4.7\text{e-}03$ | 0.996 $\pm 2.0\text{e-}03$ | 0.991 $\pm 1.2\text{e-}03$ | 0.997 $\pm 3.0\text{e-}04$ | 0.998 $\pm 1.8\text{e-}04$ |
| Estate | 0.614 ± 0.052 | 0.615 ± 0.051 | 0.614 ± 0.050 | 0.707 ± 0.062 | 0.686 ± 0.092 | 0.716 ± 0.037 | 0.762 ± 0.036 | 0.720 ± 0.058 | 0.634 ± 0.065 | 0.679 ± 0.061 |
| Housing | 0.661 $\pm 9.3\text{e-}03$ | 0.661 $\pm 9.3\text{e-}03$ | 0.660 $\pm 9.2\text{e-}03$ | 0.745 $\pm 6.7\text{e-}03$ | 0.740 $\pm 8.3\text{e-}03$ | 0.589 $\pm 8.4\text{e-}03$ | 0.747 ± 0.016 | 0.778 $\pm 7.8\text{e-}03$ | 0.796 $\pm 9.0\text{e-}03$ | 0.766 ± 0.014 |
| Infrared | 0.736 ± 0.035 | 0.740 ± 0.035 | 0.741 ± 0.033 | 0.692 ± 0.043 | 0.734 ± 0.035 | 0.761 ± 0.033 | 0.769 ± 0.031 | 0.745 ± 0.029 | 0.667 ± 0.069 | 0.725 ± 0.040 |
| Insurance | 0.738 ± 0.015 | 0.739 ± 0.015 | 0.739 ± 0.015 | 0.698 ± 0.031 | 0.849 ± 0.019 | 0.849 ± 0.015 | 0.858 ± 0.018 | 0.822 ± 0.018 | 0.806 ± 0.025 | 0.855 ± 0.013 |
| MPG | 0.803 ± 0.022 | 0.803 ± 0.023 | 0.802 ± 0.024 | 0.867 ± 0.025 | 0.818 ± 0.039 | 0.836 ± 0.025 | 0.866 ± 0.020 | 0.884 ± 0.021 | 0.846 ± 0.060 | 0.856 ± 0.030 |
| Parkinson's | 0.185 ± 0.020 | 0.185 ± 0.020 | 0.185 ± 0.020 | 0.662 ± 0.012 | 0.920 ± 0.028 | 0.462 ± 0.019 | 0.913 $\pm 6.9\text{e-}03$ | 0.614 ± 0.021 | 0.836 ± 0.058 | 0.859 ± 0.033 |
| Wine | 0.312 ± 0.017 | 0.311 ± 0.017 | 0.312 ± 0.017 | 0.358 ± 0.014 | 0.261 ± 0.019 | 0.303 ± 0.016 | 0.362 ± 0.013 | 0.378 ± 0.014 | 0.290 ± 0.029 | 0.321 ± 0.020 |
| Yacht | 0.631 ± 0.036 | 0.633 ± 0.034 | 0.645 ± 0.024 | 0.706 ± 0.049 | 0.993 $\pm 3.2\text{e-}03$ | 0.990 $\pm 3.7\text{e-}03$ | 0.995 $\pm 2.4\text{e-}03$ | 0.990 $\pm 7.4\text{e-}03$ | 0.993 $\pm 4.0\text{e-}03$ | 0.997 $\pm 1.5\text{e-}03$ |
| Mean $R^2 \uparrow$ | 0.614 | 0.615 | 0.615 | 0.727 | 0.777 | 0.725 | 0.815 | 0.781 | 0.808 | 0.810 |
| Average Rank \downarrow | 8.13 | 8.20 | 7.87 | 5.53 | 5.60 | 6.27 | 2.67 | 3.60 | 3.67 | 3.47 |

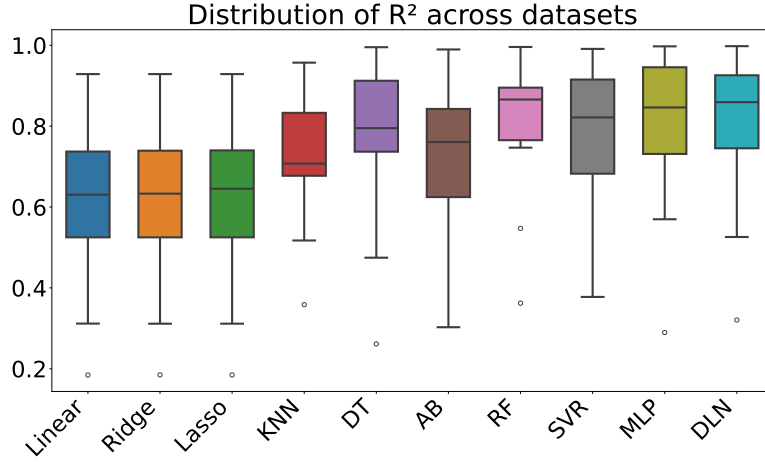


Figure 5: Distribution of R^2 across datasets for each model, averaged over 10 random seeds and 128 hyperparameter-search trials.

excels on some complex datasets but is less consistent overall. The MLP performs well on datasets that challenge most other methods (e.g., Airfoil and Bike), demonstrating its strength on highly nonlinear problems. It attains strong overall accuracy. DLN’s accuracy falls between that of random forest and the MLP.

We plot the Pearson correlation matrix of model R^2 scores in Fig. 6. A strong correlation is evident within the linear group (Linear, Ridge, Lasso) and within the tree-based group (DT, RF). DLN correlates most strongly with random forest and the MLP.

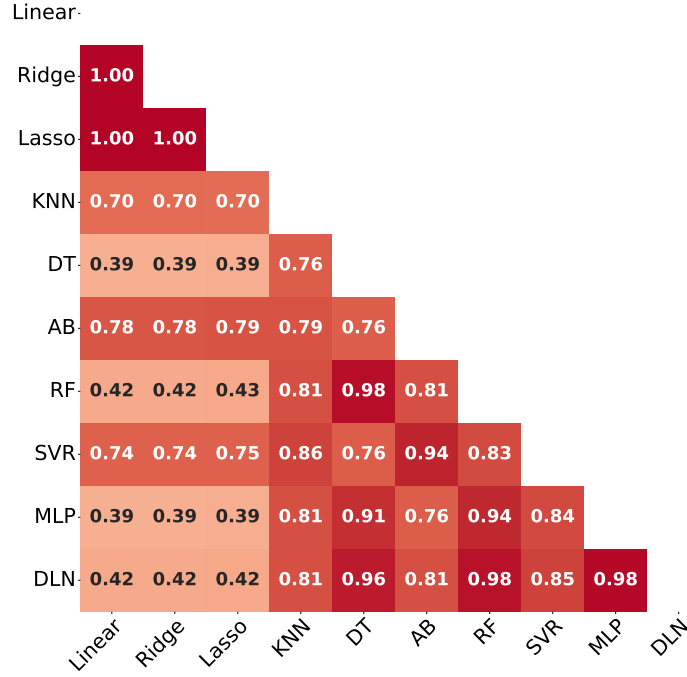


Figure 6: Pearson correlation matrix of model R^2 scores, averaged over 10 random seeds and 128 hyperparameter-search trials.

Finally, we compare performance under different hyperparameter-search budgets. Table 4 lists

each model’s average R^2 for 32, 64, and 128 trials. Nonlinear models generally improve with larger budgets; random forest benefits the most from additional trials.

Table 4: Mean R^2 scores across HPO budgets

| | 32 trials | 64 trials | 128 trials |
|--------|-----------|---------------------|---------------------|
| Linear | 0.614 | 0.614 \rightarrow | 0.614 \rightarrow |
| Ridge | 0.615 | 0.615 \rightarrow | 0.615 \rightarrow |
| Lasso | 0.615 | 0.615 \rightarrow | 0.615 \rightarrow |
| KNN | 0.726 | 0.727 \uparrow | 0.727 \rightarrow |
| DT | 0.755 | 0.771 \uparrow | 0.777 \uparrow |
| AB | 0.722 | 0.723 \uparrow | 0.725 \uparrow |
| RF | 0.793 | 0.809 \uparrow | 0.815 \uparrow |
| SVR | 0.778 | 0.781 \uparrow | 0.781 \rightarrow |
| MLP | 0.806 | 0.811 \uparrow | 0.808 \downarrow |
| DLN | 0.802 | 0.809 \uparrow | 0.810 \uparrow |

4.3 Efficiency

We follow DLN’s efficiency protocol and measure inference cost as the number of basic hardware logic-gate operations (OPs); results are shown in Table 5. Each model’s computation is first decomposed into high-level operations, such as floating-point additions and multiplications, which are then mapped to NOT, AND, OR, NAND, NOR, XOR, or XNOR gates. A two-input AND, OR, NAND, or NOR counts as one OP, a two-input XOR or XNOR as three OPs, and a NOT as zero OPs. During training, we use scikit-learn’s and PyTorch’s defaults (float32 for MLP and DLN; float64 for most traditional models), but for the cost analysis, we assume float16 for floating-point and int16 for integer arithmetic, since nearly all methods retain accuracy with these precisions. DLN involves very few floating-point calculations; hence, its relative advantage would grow if larger numeric formats were required.

From Table 5, the decision tree can be seen to be the most efficient model, followed by Lasso regression. Linear and Ridge regressions are only marginally more expensive than Lasso. DLN ranks next, with a geometric-mean inference cost $5.8\times$ lower than random forest and $86\times$ lower than the MLP.

4.4 Interpretability

A trained regression DLN can be parsed directly and its prediction expressed as a weighted collection of logic rules. Figs. 7, 8, and 9 illustrate three examples. Yellow rectangles represent input features with their learned thresholds; each outputs a binary value. Diamonds contain binary logic operators. The network’s final prediction is a weighted sum of binary rule outputs, where each rule’s coefficient is shown to the right of the edge that connects the rule node to the output node. Like their classification counterparts, regression DLNs perform implicit feature selection: in Figs. 7 and 9, only a subset of the available features is used to achieve high accuracy.

4.5 Ablation Studies

We conduct ablation studies on four design choices: temperature scheduling, unified training phases, search-space subsetting, and concatenation of ThresholdLayers to hidden LogicLayers. Table 6 reports mean results over 10 random seeds, each evaluated with 32 hyperparameter-search trials. The configuration used for the main experiments is labeled *Orig*. For context, the bottom rows of Table 6 list the R^2 and OP ranks that each ablated variant would have achieved in Tables 3 and 5.

Table 5: Average number of basic gate-level logic operations required for inference across 10 random seeds and 128 hyperparameter trials, assuming FP16 for floating-point and INT16 for integer arithmetic

| | Linear | Ridge | Lasso | KNN | DT | AB | RF | SVR | MLP | DLN |
|-----------------|--------|-------|-------|-------|-------|-------|------|-------|-------|-------|
| Abalone | 11.2K | 11.2K | 10.7K | 38.5M | 1.19K | 206K | 240K | 383M | 829K | 41.2K |
| Airfoil | 6.22K | 6.22K | 6.22K | 9.66M | 2.12K | 295K | 174K | 109M | 1.71M | 32.6K |
| Bike | 24.9K | 24.9K | 21.9K | 271M | 2.85K | 158K | 177K | 1.30G | 12.9M | 50.0K |
| CCPP | 4.98K | 4.98K | 4.98K | 38.9M | 2.01K | 199K | 201K | 504M | 1.22M | 22.5K |
| Concrete | 9.95K | 9.95K | 8.71K | 9.46M | 2.05K | 293K | 161K | 67.6M | 2.57M | 60.6K |
| Electrical | 14.9K | 14.9K | 13.3K | 89.5M | 2.36K | 296K | 191K | 1.03G | 4.65M | 91.1K |
| Energy | 12.4K | 12.4K | 11.6K | 5.55M | 1.37K | 213K | 161K | 6.73M | 2.03M | 19.8K |
| Estate | 7.46K | 7.46K | 6.47K | 1.31M | 988 | 275K | 156K | 28.5M | 962K | 12.3K |
| Housing | 14.9K | 14.9K | 14.9K | 144M | 2.58K | 207K | 207K | 1.42G | 2.14M | 49.5K |
| Infrared | 46.0K | 46.0K | 25.6K | 17.7M | 695 | 174K | 167K | 39.1M | 21.8M | 29.9K |
| Insurance | 17.4K | 17.4K | 12.9K | 16.2M | 1.15K | 94.9K | 136K | 13.6M | 801K | 5.76K |
| MPG | 9.95K | 9.95K | 8.96K | 1.78M | 1.35K | 206K | 176K | 33.6M | 2.28M | 19.6K |
| Parkinson's | 23.6K | 23.6K | 22.3K | 67.5M | 2.51K | 176K | 191K | 578M | 7.20M | 46.7K |
| Wine | 13.7K | 13.7K | 13.7K | 28.9M | 952 | 206K | 194K | 502M | 3.30M | 48.6K |
| Yacht | 7.46K | 7.46K | 1.87K | 2.20M | 1.08K | 182K | 122K | 15.9M | 1.50M | 16.7K |
| Geo. Mean OPs ↓ | 12.7K | 12.7K | 10.3K | 18.1M | 1.55K | 204K | 175K | 129M | 2.59M | 29.8K |
| Average Rank ↓ | 3.50 | 3.50 | 2.33 | 8.93 | 1.00 | 6.67 | 6.33 | 9.93 | 8.13 | 4.67 |

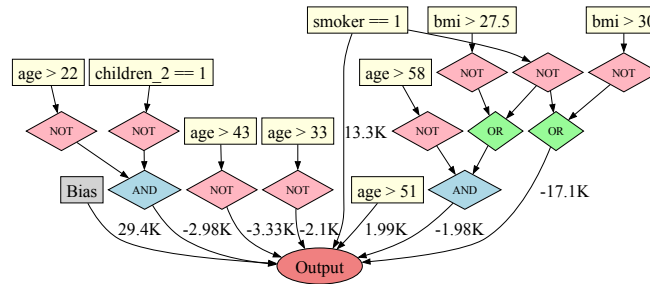


Figure 7: Decision process learned by a DLN on the *Insurance* dataset. The model attains a test R^2 of 0.866 and relies on two continuous features and two one-hot encoded categorical features, selected from an original set of two continuous and 12 one-hot features.

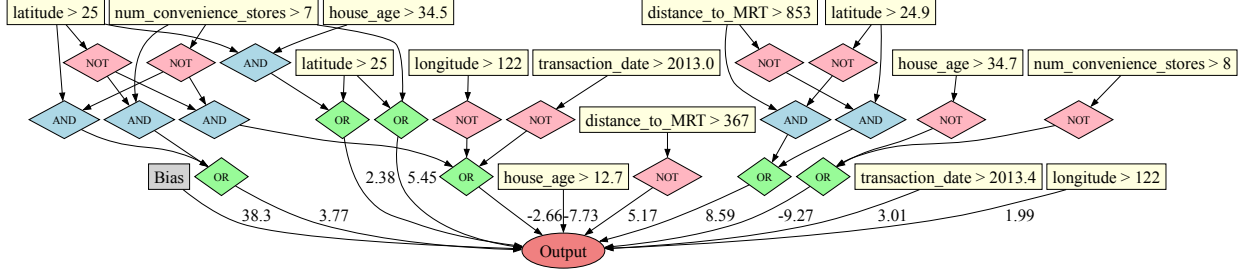


Figure 8: Decision process learned by a DLN on the *Estate* dataset. The model attains a test R^2 of 0.758 and utilizes all six continuous input features.

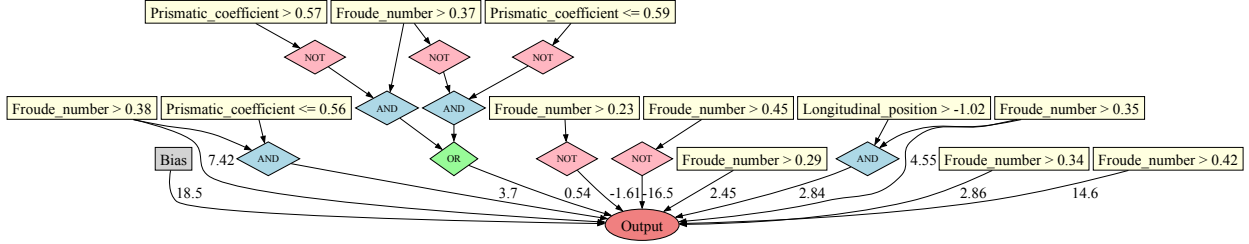


Figure 9: Decision process learned by a DLN on the *Yacht* dataset. The model attains a test R^2 of 0.997 and selects three of the six available continuous features.

Temperature scheduling. Tuning the initial temperature τ and its decay factor γ is essential; disabling this schedule markedly reduces performance.

Training phases. While the original classification DLN benefited from two distinct phases, we find that a single unified phase yields slightly better accuracy for regression DLNs.

Search-space subset. Our default setting restricts each neuron to eight logic gates and eight input links, mirroring the original DLN. Expanding to 16 gates and 16 links offers comparable accuracy, whereas shrinking to four of each degrades results.

Input concatenation. Omitting the direct concatenation of ThresholdLayer outputs to hidden LogicLayers leads to a substantial drop in accuracy.

4.6 Limitations

The main limitation of DLNs is slow training, stemming from the large number of softmax and sigmoid operations and the lack of framework-level optimizations. Even with custom CUDA kernels, the computational burden remains noticeable. Training for more epochs yields modest accuracy gains while further increasing compute cost. Furthermore, DLN and the other traditional methods lag behind the MLP on several datasets, indicating limited capacity when the target function has highly complex decision boundaries.

5 Conclusion and Future Directions

We have extended DLNs to tabular regression and shown that they preserve accuracy, interpretability, and inference efficiency in this setting. Two key training refinements, temperature scheduling and a unified single-phase optimization, further improve performance. Promising avenues for future research

Table 6: Average test R^2 for the ablation studies across 10 random seeds and 32 hyperparameter trials

| | Orig | No τ sched. | Two phases | Subspace 16 | Subspace 4 | No concat |
|---------------------------------|-------------------------------|-------------------------------|-------------------------------|-------------------------------|-------------------------------|-------------------------------|
| Abalone | 0.525 ± 0.024 | 0.524 ± 0.024 | 0.526 ± 0.027 | 0.522 ± 0.025 | 0.520 ± 0.024 | 0.514 ± 0.015 |
| Airfoil | 0.871 ± 0.021 | 0.830 ± 0.024 | 0.864 ± 0.016 | 0.874 ± 0.014 | 0.866 ± 0.015 | 0.859 ± 0.018 |
| Bike | 0.902 ± 0.016 | 0.856 ± 0.037 | 0.900 ± 0.017 | 0.911 ± 0.016 | 0.880 ± 0.017 | 0.854 ± 0.039 |
| CCPP | 0.942 $\pm 2.5\text{e-}03$ | 0.939 $\pm 2.8\text{e-}03$ | 0.941 $\pm 3.1\text{e-}03$ | 0.941 $\pm 3.0\text{e-}03$ | 0.940 $\pm 2.9\text{e-}03$ | 0.938 $\pm 2.9\text{e-}03$ |
| Concrete | 0.887 ± 0.011 | 0.866 ± 0.023 | 0.876 ± 0.016 | 0.882 ± 0.012 | 0.885 ± 0.016 | 0.873 ± 0.028 |
| Electrical | 0.926 $\pm 7.2\text{e-}03$ | 0.913 ± 0.015 | 0.932 $\pm 5.1\text{e-}03$ | 0.930 $\pm 8.6\text{e-}03$ | 0.919 $\pm 8.0\text{e-}03$ | 0.918 $\pm 5.3\text{e-}03$ |
| Energy | 0.997 $\pm 4.3\text{e-}04$ | 0.998 $\pm 2.1\text{e-}04$ | 0.997 $\pm 4.4\text{e-}04$ | 0.997 $\pm 4.8\text{e-}04$ | 0.997 $\pm 4.2\text{e-}04$ | 0.998 $\pm 5.7\text{e-}04$ |
| Estate | 0.670 ± 0.060 | 0.694 ± 0.057 | 0.669 ± 0.050 | 0.678 ± 0.063 | 0.691 ± 0.059 | 0.681 ± 0.073 |
| Housing | 0.757 ± 0.017 | 0.721 ± 0.014 | 0.754 ± 0.011 | 0.756 ± 0.019 | 0.751 ± 0.018 | 0.732 ± 0.020 |
| Infrared | 0.719 ± 0.051 | 0.723 ± 0.046 | 0.722 ± 0.027 | 0.716 ± 0.044 | 0.709 ± 0.045 | 0.701 ± 0.043 |
| Insurance | 0.854 ± 0.013 | 0.849 ± 0.015 | 0.850 ± 0.017 | 0.853 ± 0.017 | 0.852 ± 0.015 | 0.850 ± 0.016 |
| MPG | 0.856 ± 0.016 | 0.850 ± 0.022 | 0.855 ± 0.029 | 0.854 ± 0.023 | 0.843 ± 0.025 | 0.842 ± 0.029 |
| Parkinson's | 0.798 ± 0.036 | 0.690 ± 0.039 | 0.783 ± 0.024 | 0.819 ± 0.040 | 0.760 ± 0.047 | 0.649 ± 0.057 |
| Wine | 0.322 ± 0.017 | 0.330 ± 0.016 | 0.324 ± 0.023 | 0.324 ± 0.019 | 0.323 ± 0.019 | 0.326 ± 0.023 |
| Yacht | 0.997 $\pm 1.3\text{e-}03$ | 0.988 $\pm 9.9\text{e-}03$ | 0.996 $\pm 1.2\text{e-}03$ | 0.995 $\pm 3.7\text{e-}03$ | 0.996 $\pm 8.3\text{e-}04$ | 0.996 $\pm 1.7\text{e-}03$ |
| Mean $R^2 \uparrow$ | 0.802 | 0.785 | 0.799 | 0.803 | 0.795 | 0.782 |
| Average R^2 Rank \downarrow | 3.53 | 4.07 | 3.60 | 3.47 | 3.60 | 3.87 |
| Geo. Mean OPs \downarrow | 29.9K | 26.7K | 27.5K | 27.6K | 27.5K | 18.3K |
| Average OPs Rank \downarrow | 4.80 | 4.67 | 4.67 | 4.80 | 4.80 | 4.47 |

include integrating neural components into logic-based networks, as exemplified by convolutional LGN, which merges convolution and pooling operations with logical structures. Another direction is to adapt DLNs to additional data modalities, such as time series, thereby broadening their applicability.

Appendix

We plot the RMSE and MAE metrics corresponding to Table 3 in Tables 7 and 8, respectively. Across datasets, both RMSE and MAE are strongly and inversely correlated with R^2 . DLN attains the second-highest overall mean under both error measures; the MLP ranks first and random forest ranks third.

Table 7: Average test RMSE across 10 random seeds and 128 hyperparameter trials per model

| | Linear | Ridge | Lasso | KNN | DT | AB | RF | SVR | MLP | DLN |
|----------------|--------|--------|--------|--------|--------|--------|--------|----------|----------|----------|
| Abalone | 2.16 | 2.16 | 2.16 | 2.20 | 2.29 | 2.32 | 2.13 | 2.12 | 2.07 | 2.18 |
| Airfoil | 4.77 | 4.78 | 4.78 | 2.42 | 3.10 | 3.48 | 2.49 | 2.89 | 1.64 | 2.28 |
| Bike | 140 | 140 | 140 | 106 | 55.9 | 105 | 65.3 | 108 | 44.6 | 52.5 |
| CCPP | 4.54 | 4.54 | 4.54 | 3.52 | 4.11 | 4.80 | 3.90 | 3.94 | 3.86 | 4.06 |
| Concrete | 10.3 | 10.3 | 10.3 | 8.70 | 7.31 | 7.38 | 5.65 | 5.84 | 5.53 | 5.40 |
| Electrical | 0.0220 | 0.0220 | 0.0220 | 0.0166 | 0.0183 | 0.0154 | 0.0147 | 7.19e-03 | 6.57e-03 | 9.36e-03 |
| Energy | 3.00 | 3.01 | 3.01 | 2.12 | 0.676 | 1.78 | 0.639 | 0.953 | 0.513 | 0.469 |
| Estate | 7.97 | 7.97 | 7.97 | 6.91 | 7.10 | 6.82 | 6.25 | 6.75 | 7.75 | 7.25 |
| Housing | 67.1K | 67.1K | 67.1K | 58.2K | 58.8K | 73.8K | 58.0K | 54.3K | 52.0K | 55.8K |
| Infrared | 0.256 | 0.254 | 0.253 | 0.276 | 0.257 | 0.243 | 0.239 | 0.251 | 0.287 | 0.261 |
| Insurance | 6.07K | 6.06K | 6.06K | 6.51K | 4.61K | 4.61K | 4.46K | 5.00K | 5.21K | 4.52K |
| MPG | 3.49 | 3.49 | 3.51 | 2.87 | 3.35 | 3.18 | 2.88 | 2.68 | 3.05 | 2.98 |
| Parkinson’s | 9.67 | 9.67 | 9.67 | 6.23 | 2.99 | 7.86 | 3.15 | 6.65 | 4.28 | 3.99 |
| Wine | 0.718 | 0.718 | 0.718 | 0.693 | 0.744 | 0.723 | 0.691 | 0.683 | 0.729 | 0.713 |
| Yacht | 8.81 | 8.78 | 8.65 | 7.86 | 1.20 | 1.47 | 1.06 | 1.32 | 1.13 | 0.828 |
| GMean RMSE ↓ | 9.84 | 9.83 | 9.83 | 8.10 | 6.13 | 7.46 | 5.64 | 6.20 | 5.29 | 5.35 |
| Average Rank ↓ | 8.07 | 8.20 | 7.93 | 5.53 | 5.53 | 6.33 | 2.67 | 3.60 | 3.67 | 3.47 |

References

- [1] F. Petersen, C. Borgelt, H. Kuehne, and O. Deussen, “Deep differentiable logic gate networks,” in *Adv. Neural Inf. Process. Syst.*, vol. 35, 2022.
- [2] F. Petersen, H. Kuehne, C. Borgelt, J. Welzel, and S. Ermon, “Convolutional differentiable logic gate networks,” in *Adv. Neural Inf. Process. Syst.*, vol. 37, 2024.
- [3] C. Yue and N. K. Jha, “Learning interpretable differentiable logic networks,” *IEEE Trans. Circuits Syst. Artif. Intell.*, vol. 1, no. 1, pp. 69–82, 2024.
- [4] L. A. Zadeh, “Fuzzy sets as a basis for a theory of possibility,” *Fuzzy Sets Syst.*, vol. 1, no. 1, pp. 3–28, 1978.

Table 8: Average test MAE across 10 random seeds and 128 hyperparameter trials per model

| | Linear | Ridge | Lasso | KNN | DT | AB | RF | SVR | MLP | DLN |
|----------------|--------|--------|--------|--------|--------|--------|--------|----------|----------|----------|
| Abalone | 1.57 | 1.57 | 1.57 | 1.54 | 1.62 | 1.76 | 1.50 | 1.47 | 1.48 | 1.57 |
| Airfoil | 3.69 | 3.69 | 3.69 | 1.63 | 2.34 | 2.83 | 1.91 | 2.05 | 1.16 | 1.71 |
| Bike | 105 | 105 | 104 | 69.1 | 33.4 | 82.9 | 41.9 | 67.3 | 27.5 | 36.5 |
| CCPP | 3.61 | 3.61 | 3.61 | 2.48 | 3.04 | 3.76 | 2.95 | 2.95 | 2.87 | 3.09 |
| Concrete | 8.23 | 8.25 | 8.27 | 6.43 | 5.22 | 6.01 | 4.27 | 4.29 | 3.83 | 3.98 |
| Electrical | 0.0174 | 0.0174 | 0.0174 | 0.0129 | 0.0142 | 0.0126 | 0.0116 | 4.52e-03 | 4.38e-03 | 7.14e-03 |
| Energy | 2.13 | 2.13 | 2.14 | 1.39 | 0.438 | 1.47 | 0.432 | 0.722 | 0.360 | 0.347 |
| Estate | 6.07 | 6.08 | 6.06 | 4.88 | 5.16 | 4.99 | 4.43 | 4.73 | 5.51 | 5.32 |
| Housing | 48.9K | 48.9K | 48.9K | 39.0K | 39.3K | 55.8K | 40.2K | 35.9K | 35.0K | 39.1K |
| Infrared | 0.203 | 0.200 | 0.199 | 0.207 | 0.198 | 0.189 | 0.185 | 0.192 | 0.221 | 0.201 |
| Insurance | 4.24K | 4.24K | 4.21K | 3.80K | 2.15K | 2.93K | 2.52K | 2.93K | 3.12K | 2.54K |
| MPG | 2.67 | 2.67 | 2.66 | 2.05 | 2.41 | 2.33 | 2.01 | 1.89 | 2.10 | 2.15 |
| Parkinson’s | 8.03 | 8.03 | 8.04 | 3.99 | 1.41 | 6.89 | 2.10 | 4.78 | 2.54 | 2.99 |
| Wine | 0.555 | 0.556 | 0.556 | 0.538 | 0.578 | 0.571 | 0.538 | 0.524 | 0.566 | 0.552 |
| Yacht | 7.18 | 7.10 | 6.87 | 4.11 | 0.644 | 1.02 | 0.601 | 0.950 | 0.611 | 0.523 |
| GMean MAE ↓ | 7.54 | 7.53 | 7.51 | 5.52 | 4.06 | 5.75 | 3.94 | 4.34 | 3.58 | 3.84 |
| Average Rank ↓ | 8.40 | 8.33 | 8.13 | 4.80 | 5.00 | 6.73 | 2.80 | 3.33 | 3.47 | 4.00 |

- [5] K. Menger, “Statistical metrics,” *Selecta Math.*, vol. 2, pp. 433–435, 2003.
- [6] B. Goertzel, M. Iklé, I. F. Goertzel, and A. Heljakka, *Probabilistic Logic Networks: A Comprehensive Framework for Uncertain Inference*. Springer, 2008.
- [7] N. Frosst and G. Hinton, “Distilling a neural network into a soft decision tree,” in *Proc. Int. Workshop Comprehensibility & Explanation in Artif. Intell. & Mach. Learn.*, 2017.
- [8] Y. Yang, I. G. Morillo, and T. M. Hospedales, “Deep neural decision trees,” in *Proc. ICML Workshop Human Interpretability in Mach. Learn.*, 2018.
- [9] P. Kotschieder, M. Fiterau, A. Criminisi, and S. R. Buló, “Deep neural decision forests,” in *Proc. IEEE Int. Conf. Comput. Vis.*, 2015, pp. 1467–1475.
- [10] R. Tanno, K. Arulkumaran, D. Alexander, A. Criminisi, and A. Nori, “Adaptive neural trees,” in *Proc. Int. Conf. Mach. Learn.*, 2019, pp. 6166–6175.
- [11] S. Popov, S. Morozov, and A. Babenko, “Neural oblivious decision ensembles for deep learning on tabular data,” in *Proc. Int. Conf. Learn. Represent.*, 2020.
- [12] Z. Liu, Y. Wang, S. Vaidya, F. Ruehle, J. Halverson, M. Soljačić, T. Y. Hou, and M. Tegmark, “KAN: Kolmogorov-Arnold networks,” in *Proc. Int. Conf. Learn. Represent.*, 2025.
- [13] M. Raissi, P. Perdikaris, and G. E. Karniadakis, “Physics-informed neural networks: A deep learning framework for solving forward and inverse problems involving nonlinear partial differential equations,” *J. Comput. Phys.*, vol. 378, pp. 686–707, 2019.

- [14] Y. Hu, L. Anderson, T.-M. Li, Q. Sun, N. Carr, J. Ragan-Kelley, and F. Durand, “DiffTaichi: Differentiable programming for physical simulation,” in *Proc. Int. Conf. Learn. Represent.*, 2020.
- [15] M. Cranmer, A. Sanchez Gonzalez, P. Battaglia, R. Xu, K. Cranmer, D. Spergel, and S. Ho, “Discovering symbolic models from deep learning with inductive biases,” in *Adv. Neural Inf. Process. Syst.*, vol. 33, 2020, pp. 17 429–17 442.
- [16] A. G. Baydin, B. A. Pearlmutter, A. A. Radul, and J. M. Siskind, “Automatic differentiation in machine learning: A survey,” *J. Mach. Learn. Res.*, vol. 18, no. 153, pp. 1–43, 2018.
- [17] F. Petersen, “Learning with differentiable algorithms,” Ph.D. dissertation, University of Konstanz, 2022.
- [18] M. Cuturi and M. Blondel, “Soft-DTW: A differentiable loss function for time-series,” in *Proc. Int. Conf. Mach. Learn.*, 2017, pp. 894–903.
- [19] M. T. Ribeiro, S. Singh, and C. Guestrin, ““Why should I trust you?” Explaining the predictions of any classifier,” in *Proc. ACM SIGKDD Int. Conf. Knowl. Discov. Data Min.*, 2016, pp. 1135–1144.
- [20] S. M. Lundberg and S.-I. Lee, “A unified approach to interpreting model predictions,” in *Adv. Neural Inf. Process. Syst.*, vol. 30, 2017.
- [21] K. Simonyan, A. Vedaldi, and A. Zisserman, “Deep inside convolutional networks: Visualising image classification models and saliency maps,” in *Proc. Int. Conf. Learn. Represent., Workshop Track*, 2014.
- [22] C. Olah, A. Mordvintsev, and L. Schubert, “Feature visualization,” *Distill*, vol. 2, no. 11, p. e7, 2017.
- [23] A. Goldstein, A. Kapelner, J. Bleich, and E. Pitkin, “Peeking inside the black box: Visualizing statistical learning with plots of individual conditional expectation,” *J. Comput. Graph. Stat.*, vol. 24, no. 1, pp. 44–65, 2015.
- [24] C. Rudin, “Stop explaining black box machine learning models for high stakes decisions and use interpretable models instead,” *Nat. Mach. Intell.*, vol. 1, no. 5, pp. 206–215, 2019.
- [25] A. E. Hoerl and R. W. Kennard, “Ridge regression: Biased estimation for nonorthogonal problems,” *Technometrics*, vol. 12, no. 1, pp. 55–67, 1970.
- [26] R. Tibshirani, “Regression shrinkage and selection via the Lasso,” *J. R. Statist. Soc. Series B Methodol.*, vol. 58, no. 1, pp. 267–288, 1996.
- [27] T. J. Hastie, “Generalized additive models,” in *Statistical Models in S*. Routledge, 2017, pp. 249–307.
- [28] J. H. Friedman and B. E. Popescu, “Predictive learning via rule ensembles,” *Ann. Appl. Stat.*, vol. 2, no. 3, pp. 916–954, 2008.
- [29] J. Lin, C. Zhong, D. Hu, C. Rudin, and M. Seltzer, “Generalized and scalable optimal sparse decision trees,” in *Proc. Int. Conf. Mach. Learn.*, 2020, pp. 6150–6160.
- [30] B. Ustun and C. Rudin, “Supersparse linear integer models for optimized medical scoring systems,” *Mach. Learn.*, vol. 102, pp. 349–391, 2016.

- [31] R. Riegel, A. Gray, F. Luus, N. Khan, N. Makondo, I. Y. Akhalwaya, H. Qian, R. Fagin, F. Barahona, U. Sharma *et al.*, “Logical neural networks,” *arXiv preprint arXiv:2006.13155*, 2020.
- [32] Z. Wang, W. Zhang, N. Liu, and J. Wang, “Scalable rule-based representation learning for interpretable classification,” in *Adv. Neural Inf. Process. Syst.*, vol. 34, 2021.
- [33] H. Dong, J. Mao, T. Lin, C. Wang, L. Li, and D. Zhou, “Neural logic machines,” in *Proc. Int. Conf. Learn. Represent.*, 2019.
- [34] S. Shi, H. Chen, M. Zhang, and Y. Zhang, “Neural logic networks,” *arXiv preprint arXiv:1910.08629*, 2019.
- [35] S. Han, J. Pool, J. Tran, and W. Dally, “Learning both weights and connections for efficient neural network,” in *Adv. Neural Inf. Process. Syst.*, vol. 28, 2015.
- [36] J. Frankle and M. Carbin, “The lottery ticket hypothesis: Finding sparse, trainable neural networks,” in *Proc. Int. Conf. Learn. Represent.*, 2019.
- [37] M. Courbariaux, I. Hubara, D. Soudry, R. El-Yaniv, and Y. Bengio, “Binarized neural networks: Training deep neural networks with weights and activations constrained to +1 or -1,” in *Adv. Neural Inf. Process. Syst.*, vol. 29, 2016.
- [38] M. Rastegari, V. Ordonez, J. Redmon, and A. Farhadi, “XNOR-Net: Imagenet classification using binary convolutional neural networks,” in *Proc. Eur. Conf. Comput. Vis.*, 2016, pp. 525–542.
- [39] E. Frantar, S. Ashkboos, T. Hoeffler, and D. Alistarh, “GPTQ: Accurate post-training quantization for generative pre-trained transformers,” in *Proc. Int. Conf. Learn. Represent.*, 2023.
- [40] Y. Zhao, C.-Y. Lin, K. Zhu, Z. Ye, L. Chen, S. Zheng, L. Ceze, A. Krishnamurthy, T. Chen, and B. Kasicki, “Atom: Low-bit quantization for efficient and accurate LLM serving,” in *Proc. Mach. Learn. Syst.*, vol. 6, 2024, pp. 196–209.
- [41] G. Hinton, O. Vinyals, and J. Dean, “Distilling the knowledge in a neural network,” in *Proc. Neural Inf. Process. Syst. Deep Learn. & Represent. Learn. Workshop*, 2015.
- [42] Y. Gu, L. Dong, F. Wei, and M. Huang, “MiniLLM: Knowledge distillation of large language models,” in *Proc. Int. Conf. Learn. Represent.*, 2023.
- [43] Y. Umuroglu, N. J. Fraser, G. Gambardella, M. Blott, P. Leong, M. Jahre, and K. Vissers, “FINN: A framework for fast, scalable binarized neural network inference,” in *Proc. ACM/SIGDA Int. Symp. Field-Program. Gate Arrays*, 2017, pp. 65–74.
- [44] Y. Bengio, N. Léonard, and A. Courville, “Estimating or propagating gradients through stochastic neurons for conditional computation,” *arXiv preprint arXiv:1308.3432*, 2013.
- [45] H.-T. Cheng, L. Koc, J. Harmsen, T. Shaked, T. Chandra, H. Aradhye, G. Anderson, G. Corrado, W. Chai, M. Ispir *et al.*, “Wide & deep learning for recommender systems,” in *Proc. 1st Workshop Deep Learn. Recommender Syst.*, 2016.
- [46] A. Meurer, C. P. Smith, M. Paprocki, O. Čertík, S. B. Kirpichev, M. Rocklin, A. Kumar, S. Ivanov, J. K. Moore, S. Singh, T. Rathnayake, S. Vig, B. E. Granger, R. P. Muller, F. Bonazzi, H. Gupta, S. Vats, F. Johansson, F. Pedregosa, M. J. Curry, A. R. Terrel, v. Roučka, A. Saboo, I. Fernando, S. Kulal, R. Cimrman, and A. Scopatz, “SymPy: Symbolic computing in Python,” *PeerJ Comput. Sci.*, vol. 3, p. e103, Jan. 2017. [Online]. Available: <https://doi.org/10.7717/peerj-cs.103>

- [47] M. Kelly, R. Longjohn, and K. Nottingham, “The UCI machine learning repository,” <https://archive.ics.uci.edu>, accessed: May 01, 2025.
- [48] Kaggle, “Kaggle,” <https://www.kaggle.com>, accessed: May 01, 2025.
- [49] T. Akiba, S. Sano, T. Yanase, T. Ohta, and M. Koyama, “Optuna: A next-generation hyperparameter optimization framework,” in *Proc. ACM SIGKDD Int. Conf. Knowl. Discov. Data Min.*, 2019, pp. 2623–2631.
- [50] F. Pedregosa, G. Varoquaux, A. Gramfort, V. Michel, B. Thirion, O. Grisel, M. Blondel, P. Prettenhofer, R. Weiss, V. Dubourg *et al.*, “Scikit-learn: Machine learning in Python,” *J. Mach. Learn. Res.*, vol. 12, pp. 2825–2830, 2011.
- [51] A. Paszke, S. Gross, F. Massa, A. Lerer, J. Bradbury, G. Chanan, T. Killeen, Z. Lin, N. Gimelshein, L. Antiga *et al.*, “Pytorch: An imperative style, high-performance deep learning library,” in *Adv. Neural Inf. Process. Syst.*, vol. 32, 2019.
- [52] P. Moritz, R. Nishihara, S. Wang, A. Tumanov, R. Liaw, E. Liang, M. Elibol, Z. Yang, W. Paul, M. I. Jordan *et al.*, “Ray: A distributed framework for emerging AI applications,” in *Proc. USENIX Symp. Oper. Syst. Des. Implement.*, 2018, pp. 561–577.